Title

Quantitative MRI Musculoskeletal Techniques: An Update.

Journal

American Journal of Roentgenology, 213(3)

ISSN

0361-803X

Authors

de Mello, Ricardo
Ma, Yajun
Ji, Yang
et al.

Publication Date

2019-09-01

DOI

10.2214/ajr.19.21143

Peer reviewed

AJR FOCUS ON:

Quantitative MRI Musculoskeletal Techniques: An Update

Ricardo de Mello[1,2]
Yajun Ma[1]
Yang Ji[1]
Jiang Du[1]
Eric Y. Chang[1,3]

OBJECTIVE. For many years, MRI of the musculoskeletal system has relied mostly on conventional sequences with qualitative analysis. More recently, using quantitative MRI applications to complement qualitative imaging has gained increasing interest in the MRI community, providing more detailed physiologic or anatomic information.

CONCLUSION. In this article, we review the current state of quantitative MRI, technical and software advances, and the most relevant clinical and research musculoskeletal applications of quantitative MRI.

Keywords: MRI, musculoskeletal, quantitative imaging

doi.org/10.2214/AJR.19.21143

Received January 12, 2019; accepted after revision February 25, 2019.

The opinions and assertions contained herein are the private views of the authors and are not to be construed as official or as representing the views of the Department of Veterans Affairs.

Supported by Merit Awards I01CX001388 and I01RX002604 from the U.S. Department of Veterans Affairs, grants 1R21AR073496, R01AR068987, and 5R01AR062581 from the National Institutes of Health, and support from GE Healthcare.

[1]Department of Radiology, University of California, San Diego Medical Center, San Diego, CA.

[2]Department of Internal Medicine, Federal University of Espírito Santo, Vitória, Brazil.

[3]Radiology Service, VA San Diego Healthcare System, 3350 La Jolla Village Dr, MC 114, San Diego, CA 92161. Address correspondence to E. Y. Chang (ericchangmd@gmail.com)

AJR 2019; 213:524–533

0361–803X/19/2133–524

MRI has been shown to be a very helpful tool in the diagnosis of many musculoskeletal (MSK) disorders and has been established as a very reliable modality for noninvasive evaluation of the MSK system, thereby becoming an indispensable clinical diagnostic tool [1, 2]. Most clinical MRI requests are for evaluation of connective tissue pathologic abnormalities, such as meniscal tears, rotator cuff tears, and ligament and tendon lesions. MSK MRI protocols have been tailored to accommodate this scenario.

For many years, MRI of the MSK system has relied mostly on conventional sequences with qualitative analysis. The rate of MRI studies and MSK applications keeps expanding [3], and lately, quantitative MRI (QMRI) applications are gaining interest in the MRI community. QMRI can complement qualitative imaging with more detailed physiologic or anatomic information, providing measures that could aid in earlier disease detection, comparative studies, and monitoring treatment [4]. However, despite recent advances, technical challenges and specific recommendations for QMRI must be taken into consideration.

In this article, we review new developments in QMRI, technical and software advances, and the most relevant clinical and research MSK applications of QMRI. In particular, we focus on quantitative techniques that are currently available or are among the most promising for clinical use.

T2 Mapping

Different MRI parametric mapping techniques are available, such as T2, T2*, and T1 mapping, but the most widely available and frequently obtained is T2 mapping. This technique typically requires acquisition of multiple images with different TEs that will yield signal intensities that follow a T2 relaxation curve, such as with the single-echo spin-echo, multiecho spin-echo, and double-echo steady-state sequences [5, 6]. When implementing T2 mapping in clinical practice, considerations should be given to acquisition, postprocessing, and interpretation.

Acquisition of T2-mapping techniques can be lengthy, and patient motion during the sequence can result in inaccurate mapping. In addition, a technical challenge that can be seen with some parametric mapping techniques, such as multiecho spin-echo T2 mapping, is sensitivity to B_1 inhomogeneity [7]. B_1 inhomogeneity is particularly prominent at high field strengths, such as 3 T, and can lead to inaccuracies in quantification. Different T2-mapping methods have been proposed to overcome this limitation, including the use of a T2-preparation pulse to ensure B_1 insensitivity, followed by either a gradient-echo readout or 3D turbo spin-echo readout [8]. The T2-preparation pulse consists of a spin-echo–like preparation pulse to transmit the T2-weighted contrast and a readout design for fast image data gathering. T2-preparation techniques have faster acquisition times than the multiecho spin-echo technique, but they

acquire fewer echoes and, therefore, provide fewer data points along the T2 decay curve, with possible compromise in the accuracy of T2 values [9].

Postprocessing of the multiple images generated by the T2-mapping sequences can be performed online on the scanner or offline using algorithms written in separate programs, such as MATLAB (Mathworks). Automated processing on the scanner typically generates a pixel-by-pixel map of T2 relaxation times, with a scale bar based on the range of values in the FOV. With offline processing, additional steps can be performed, including image registration, segmentation of structures, and selection of ROIs to generate fitting curves, which can be used to assess the quality of the data (Fig. 1). Interpretation of T2 values and visual maps requires many considerations. First, care must be taken when comparing absolute T2 relaxation times, because values may differ depending on anatomic location [10], with the highest values typically seen at the magic angle [11] (Fig. 1). In addition, values can vary depending on the scanner and sequence used for acquisition. However, abrupt changes or irregularities, which may be highlighted on T2 maps, can be considered abnormal. Despite the challenges, T2 mapping remains useful in clinical practice and has been validated for noninvasive quantitative analysis of tissue composition and structure. T2 mapping can be easily implemented on most clinical MRI systems and has the advantage of not requiring contrast agent administration [12].

T2 maps can be used for quantitative evaluation of nearly any MSK tissue, but the most frequent use is for the assessment of articular hyaline cartilage. For cartilage, density and organization of the extracellular matrix appear as variations of T2 values that can be represented by either a gray-scale or color map [13]. T2 mapping has been shown to be effective in detecting and quantifying early changes related to water content and collagen concentration, even before detectable structural changes occur [14, 15]. It can be applied to identify early stage degeneration and cartilage with irreversible damage [16, 17], to assess functional potential, study reparative tissue, or monitor the effects of chondroprotective therapy [18, 19].

T2 maps can also be used for evaluation of muscle composition, especially for quantification of edema and inflammatory changes [20]. A challenge with muscle T2 mapping is the effect of fatty degeneration on T2 values, because both edema or inflammatory changes and fatty degeneration lead to increased T2 values [21, 22]. These effects should be considered when evaluating patients with inflammatory myopathies and neuromuscular disorders, because patients can show concomitant findings of muscle edema and fatty infiltration [23]. Interpretation of T2 mapping in these scenarios requires careful analysis because of the multiple factors affecting T2 values [24, 25]. To reduce the effect of fat content on T2 maps, the implementation of fat-suppression techniques is an alternative [26], despite recognized limitations for the complete removal of the fat content effect on T2 values [27]. The use of both fat-saturated and non–fat-saturated acquisitions can help analyze the specific findings in muscle T2 maps [26]. Fat infiltration in obese patients and muscle edema related to exercise are also confounding factors that can contribute to elevated T2 values and need to be taken into consideration when evaluating muscle T2 maps [25, 28]. Overall, T2 mapping can be very useful in clinical practice, but the radiologist should be aware of the potential challenges because standardized T2 measurement protocols are absent, which make meta-analyses and multisite comparison difficult.

T1ρ Mapping

T1ρ, also referred to as T1rho or spin-lock relaxation, is another technique used to evaluate biochemical changes in tissues. T1ρ is the time constant of spin-lattice relaxation in the rotating frame, characterized by magnetic relaxation of spins under the influence of a radiofrequency pulse. It is sensitive for low-frequency interactions between macromolecules and bulk water [29, 30]. T1ρ is similar to T2 relaxation, except that there is an additional radiofrequency pulse (the spin-locking pulse) applied immediately after the magnetization is tipped into the transverse plane. Conventionally, the spin-locking pulse is a continuous wave radiofrequency pulse with long duration and low energy. Because the magnetization and radiofrequency field are along the same direction, this effectively locks the magnetization vector into the transverse plane without phase decay (as with T2 decay). The signal decay is exponential with a time constant, T1ρ, and is typically calculated from multiple images by changing the duration of the spin-locking pulse. Changing the amplitude of the spin-locking pulse can also select for different properties within the tissue [5, 29, 31]. Because the conventional continuous wave spin-locking pulse is susceptible to field inhomogeneities, recent studies have evaluated techniques using adiabatic T1ρ spin-locking pulses, where amplitude and frequency are varied in time, showing promising results in osteoarthritis, with reduction of the effects of magnetic field inhomogeneities and also reduced sensitivity to the magic angle effect [32, 33].

Several studies have shown that T1ρ imaging is sensitive to detecting changes in proteoglycan content of articular cartilage, as found in the early stages of osteoarthritis [29, 34, 35]. T1ρ has also been shown to be reliable in mapping cartilage damage in patients with rheumatoid arthritis and osteoarthritis [36]. T1ρ depicts changes between protons and the macromolecular environment of cartilage. Considering that the motion of water molecules in articular cartilage is restricted by the macromolecules in the extracellular matrix, alterations such as proteoglycan loss can, therefore, be reflected in T1ρ values [5, 34, 37]. In comparison with other techniques, T1ρ mapping has the advantage of providing noninvasive analysis of proteoglycan content in cartilage without the need for contrast agent administration or any extra hardware [35] (Fig. 2). However, it requires a pulse sequence that is not widely available. Other limitations of T1ρ mapping are related to variability of results between different pulse sequences [38] and the angular and layer dependence of T1ρ values [39]. T1ρ measurements can also be confounded by the presence of multiple tissue components [40].

Delayed Gadolinium-Enhanced MRI of Cartilage

Delayed gadolinium-enhanced MRI of cartilage (dGEMRIC) provides indirect measurement of cartilage structural composition and is based on the inverse relationship between cartilage glycosaminoglycan (GAG) content and cartilage distribution of the negatively charged gadolinium contrast agent [41]. GAG molecules play an important role in cartilage integrity by helping keep water molecules within cartilage and, therefore, maintaining swelling pressure and strength. A decrease in GAG molecules in the cartilage is one of the early steps of osteoarthritis development.

GAG molecules and gadolinium are both negatively charged, and gadolinium will accumulate in articular cartilage in an inversely proportional manner to the GAG concentration: in areas with decreased GAG concentration (i.e., lesser negative charge), more negatively charged gadolinium will penetrate the cartilage. Images are generally obtained 90–120 minutes after IV injection of contrast agent to allow its diffusion

within the cartilage. dGEMRIC is based on a T1 relaxation time measurement technique that uses the negative ionic charge of gadolinium to generate a color-coded map of the charge density of cartilage GAGs [42]. Accumulation of the contrast agent in areas of low GAG content in the cartilage will result in shorter T1 relaxation time.

dGEMRIC maps can reliably detect GAG loss even before conventional MRI can detect cartilage changes. Different studies have shown that dGEMRIC is a valuable noninvasive tool in the evaluation of cartilage changes, as is seen in early stage osteoarthritis and focal cartilage defects [41, 43, 44], femoroacetabular joint disorders [45], follow-up of surgically treated cartilage [46], and injured joints after dislocations and ligament tears [47, 48]. In osteoarthritis research studies, dGEMRIC has been used as a standard tool for the assessment of articular cartilage GAG [41, 49].

Practical limitations of this technique are the prolonged acquisition protocol due to the long delay between the contrast agent administration and MRI acquisition, the lack of a standard physical activity protocol required before image acquisition, and the increased costs and risks associated with IV administration of contrast agent [42, 49].

Proton MR Spectroscopy

In vivo proton MR spectroscopy (MRS) offers noninvasive molecular characterization of different tissues, sampling the relative levels of metabolites in specific ROIs [50]. MRS has been used successfully to study the intracellular contents of skeletal muscle tissue, monitoring such metabolites as choline, lipids, total creatine, and trimethyl ammonium [51] (Fig. 3). However, compared with other body regions, such as the brain, MRS has had rather restricted applications in the MSK system.

Multiple studies have used MRS for characterization of MSK tumors. By quantitatively assessing choline content, differentiation between benign and malignant lesions is possible [52, 53]. Another application of MRS is to quantify skeletal muscle lipid storage, evaluating both intramyocellular and extramyocellular lipid compartments [54]. Muscular lipid metabolism measurements offer an ample spectrum of clinical and research applications for MRS, including correlations to exercise physiology, muscular function, insulin resistance, obesity, and other metabolic disorders [55–59]. Muscle metabolites other than lipids, such as creatine, have also been evaluated, providing a potential avenue to improve understanding of muscle metabolism and to monitor response to therapies [60].

Specific MRS techniques, such as ^{31}P-MRS, require specialized MRI hardware, which limits their clinical adequacy. Proton MRS, on the other hand, does not involve special hardware and can, therefore, be performed as part of routine MRI. However, MRS measurements are affected by many imaging-related factors. One described limitation of muscle MRS is related to the reliance on ratios between water and fat or metabolite content and to the assumption of consistent water content within muscle, which can lead to inaccurate measurements in patients who present with both muscle edema or inflammation and fatty degeneration, such as patients with dystrophinopathies [61].

Chemical-Shift MRI

MRI allows quantification of fatty infiltration using several approaches, including chemical-shift water-fat MRI, which relies on the difference in chemical shift between water and fat, enabling assessment and quantification of the fatty elements in muscle tissue using fat fraction maps [62, 63] (Fig. 4). Chemical-shift imaging (CSI), proposed by Dixon in 1984 [64], uses the phenomenon of signal intensity alterations detected in MRI that result from the inherent differences in the resonant frequencies of lipid and water. These differences can be encoded into images, producing sets of images based on water and fat. Fat and water signals can then be used to calculate the fat fraction, expressed as the fraction of fat signal in the total signal in each voxel [65].

CSI methods have been applied mostly to quantify fat replacement of skeletal muscle. Fat fractions obtained by CSI have been shown to correlate well with histologic examination and MRS [66]. Two- and three-point Dixon imaging have shown good correlations with fat levels based on muscle biopsy and clinical severity in dystrophinopathies [67, 68]. It has also been applied to provide outcome measures and to detect disease progression [69].

In comparison with signal intensity approaches, CSI methods are less influenced by B_0 and B_1 magnetic field inhomogeneities and are less biased by partial volume effects [66]. However, it has been suggested that low signal-to-noise ratio images affect the accuracy of the results, especially when one of the components is predominant—namely, low fat fraction or low water fraction [70]. Another challenge to CSI is related to the definition of ROIs and delineation of muscle contours. Manual segmentation is very time consuming, and recent advances in semiautomatic or automatic segmentation are still difficult to apply in the clinical setting. Faster and simpler automated or semiautomated muscle segmentation would be highly beneficial for the analysis of quantitative muscle MRI [71].

DWI

DWI is an MRI technique capable of measuring differences in the magnitude of diffusion of water molecules within a tissue [72]. DWI is an established technique in neuroradiology but has not been widely used for MSK imaging, although promising applications have been studied [73]. DWI generates MR images on the basis of the contrast derived from the diffusion property of water molecules, thereby allowing mapping of the diffusion process that will reflect the difference in rate of diffusion in tissues. Diffusion, also known as Brownian motion, denotes the random thermal movement of molecules. Diffusion of water molecules follows a pattern according to each tissue composition and structure, and some pathologic conditions can alter this diffusion, allowing abnormalities to be detected by DWI [74, 75]. DWI can be generated by applying two extra diffusion gradients, equal in magnitude, on conventional MRI sequences—one dephasing and one, exactly opposite, rephasing gradient. The first gradient introduces phase shift to the molecules, whereas the second gradient will cancel these changes. With diffusion of protons, the second gradient is not able to completely reverse the changes induced by the first gradient on moving spins, and signal attenuation can be detected. The detected signal loss is related to the resultant spin dephasing, varying according to time between pulses, strength, and duration of gradients applied. Apparent diffusion coefficient maps can then be obtained, derived from at least two DW images, displaying the spatial distribution of the different diffusion rates. Apparent diffusion coefficient maps also reduce T1 and T2 contrast in the images and allow diffusion quantification [74, 75].

For muscle MRI, although conventional sequences are sensitive to detect larger abnormalities, edema, and hemorrhage, DWI can help detect minor lesions and fatigue-induced muscle disorders that would otherwise remain undetected, thus improving diagnosis [76]. DWI can also be combined with the diffusion-tensor imaging (DTI) technique. Considering that the diffusion of molecules in structured tissue is anisotropic, DTI parameters can be used to measure anisotropy, to allow noninvasive evaluation of tissue microstructure and mechanical

properties, and to map the orientation of skeletal muscle fibers [73, 77]. DTI is able to measure the magnitude and direction of mobility of molecules in a particular voxel and can become a useful tool for investigation of muscle disorders. DTI measurements allow calculation of parameters for overall diffusivity and for the degree of anisotropy (fractional and relative anisotropy) [78]. Certain conditions, such as mechanical injury and exercise-related trauma, can lead to disorganization of muscle fibers and altered diffusion, with consequent decreased anisotropy, that can sometimes be detected even before it becomes apparent on conventional images, helping with early diagnosis and definition of the lesion extension [76, 79]. DTI can be applied to study skeletal muscle physiology, anatomy, and pathology and could become diagnostically relevant for prognosis and treatment of sports-related muscle injury [76, 80]. However, DWI and DTI are dependent on many acquisition parameters and are prone to artifacts from misregistration of data, motion artifacts, and susceptibility variants. Muscle DTI parameters are also highly sensitive to age, sex, body mass index, exercise status, and temperature [80]. Further research is necessary, and improvements in the technique and in postprocessing analysis are needed to increase the application in both research and clinical medicine [73].

Ultrashort- and Zero-TE Sequences

Tendons, ligaments, menisci, and bones contain a high fraction of components with short and ultrashort transverse relaxation times and, therefore, have short mean transverse relaxation times [81]. These tissues yield little or no signal with conventional MRI pulse sequences and, thus, are not able to be properly characterized using these sequences with longer TEs. Tendons, ligaments, and menisci have T2 times of 2–8 ms, and cortical bone and the deep layers of articular cartilage have T2 times of about 0.2–2 ms [81]. To detect and explore signals from these tissues with very short T2 times, which are especially relevant in the MSK system, different ultrashort-TE (UTE) and zero-TE sequences have been designed. They are being increasingly improved and studied, thus providing the opportunity to visualize and detect abnormalities of these tissues in a manner not previously possible [81–85] (Fig. 2).

Ultrashort-TE T2 Mapping*

UTE T2* mapping, similar to quantitative conventional T2* mapping, is based on a series of multiple images at different TEs, including TE of 0.5 ms or shorter [86]. T2* is the most popular relaxation constant used to detect potential collagen matrix alteration in tendons [87]. The number of components and T2* values vary according to spatial resolution and tendon orientation [88]. Biexponential T2* analysis has been successfully performed in vivo using both UTE and variable TE sequences, and fractions and T2* values vary depending on tendon location, which is consistent with different tendon compositions [81]. Recent studies have shown that biexponential T2* offers robust measurements in both healthy individuals and patients with Achilles and patellar tendinopathy [83, 89, 90]. UTE T2* can become a reliable marker to guide clinical outcome, detecting tendinopathy. Bicomponent analysis can also be useful in quantifying the injured or postoperative tendon (Fig. 4). T2* limitations are related to magnetic field inhomogeneities and magic angle effects.

UTE and zero-TE techniques can obtain signal from the short T2* components of articular cartilage, allowing direct visualization of the deep layers and discrimination of the calcified layer, which may be related to the pathogenesis of cartilage degeneration [91, 92] (Fig. 5). Conventional MRI sequences cannot differentiate the deep radial and calcified layers from subchondral bone [93]. Williams et al. [86], using a monoexponential decay model, found that UTE T2* values were more sensitive to matrix degeneration than conventional T2 values based on histologic standards, showing lower UTE T2* values associated with severely degraded cartilage. In a recent study of patients 2 years after anterior cruciate ligament reconstruction, UTE T2* assessment could identify deep articular pathologic abnormalities in subclinical disease that were not evident at conventional MRI [94]. Chu et al. [95] showed that UTE T2* values were significantly elevated in patients who had undergone ACL reconstruction with arthroscopically normal articular cartilage and menisci. Shao et al. [96] recently found that UTE bicomponent analysis can characterize the short and long T2* values and fractions across the cartilage depth, including the deep radial and calcified cartilage.

UTE T2* can also be used to assess bone. For cortical bone, recent studies have shown that biexponential T2* fitting and adiabatic inversion recovery UTE techniques can reliably measure bound water and pore water components in vitro and in vivo [84, 97, 98]. Future studies can confirm the potential of these techniques to assess bone quality and strength and to determine its implications for clinical evaluation of bone diseases. Challenges related to UTE T2* are the lack of availability on most existing scanners, additional cost, and extra clinical examination times, because it will need to be performed in addition to clinical sequences. For clinical imaging, limitations related to imperfect registration and patient motion may affect measurements [99]. Another source of potential limitations can be related to issues in the processing of exponential fitting of multiecho images [40].

Ultrashort-TE Magnetization Transfer

For certain anisotropic tissues, such as tendons and cortical bone, low mean transverse relaxation time is not the only challenge for imaging. An additional concern is the magic angle effect, which is related to unaveraged dipolar interactions of proton nuclear spins [100]. Magnetization transfer (MT) refers to the interactions of protons residing in different macromolecular environments and the transfer of longitudinal magnetization from the bound proton pool to the free proton pool. When combined with the UTE sequence, MT can be performed on short-T2 tissues [101]. UTE MT may provide unique information that cannot be directly obtained by other methods, such as regular UTE techniques, and multiple parameters can be obtained, including water and macromolecular proton fractions, as well as relaxation and exchange rates [102]. UTE MT with two-pool modeling measurements has shown much less orientational dependence and has shown potential as a clinically compatible quantitative technique that is resistant to the magic angle effect [103]. However, UTE MT protocols with relatively small saturation pulses may lead to inaccuracy in the measurement of T2 of the water pool, which is related to underestimation of the exchange rate between macromolecular and water pools [103]. In addition, the two-pool model does not account for the presence of fat, which would confound the measurements. Fat-saturation methods or a three-pool model could be used in future studies.

Recent studies using the UTE MT technique on rotator cuff tendons have shown promising results that are much less sensitive to magic angle effects compared with transverse relaxation times [103, 104] (Fig. 6). For cortical bone, studies by Chang et al. [105] and Ma et al. [106] found encouraging results investigating 2D UTE MT that can provide useful quantification information for cortical bone (Fig. 7).

Conclusion

MRI is continuously being refined, and an ample range of quantitative sequences and techniques are now available, enabling the visualization of previously invisible structures and characterization of multiple MSK tissues. However, many of the newer QMRI techniques are not widely available in clinical packages or cannot be performed during clinically feasible scan times, and specific recommendations are not adopted because of the lack of standardization and validation, especially across different equipment and systems. Further refinements are needed to facilitate and speed up its adoption, making it easier to compare its results over time, between subjects and with different equipment.

References

1. Ahn JM, El-Khoury GY. Role of magnetic resonance imaging in musculoskeletal trauma. *Top Magn Reson Imaging* 2007; 18:155–168
2. Mosher TJ. Musculoskeletal imaging at 3T: current techniques and future applications. *Magn Reson Imaging Clin N Am* 2006; 14:63–76
3. Solomon DH, Katz JN, Carrino JA, et al. Trends in knee magnetic resonance imaging. *Med Care* 2003; 41:687–692
4. Xiao L, Yuen MK. State-of-the-art musculoskeletal magnetic resonance imaging: technical review. *Hong Kong J Radiol* 2017; 20:6–16
5. Li X, Majumdar S. Quantitative MRI of articular cartilage and its clinical applications. *J Magn Reson Imaging* 2013; 38:991–1008
6. Staroswiecki E, Granlund KL, Alley MT, Gold GE, Hargreaves BA. Simultaneous estimation of T_2 and ADC in human articular cartilage *in vivo* with a modified 3D DESS sequence at 3 T. *Magn Reson Med* 2012; 67:1086–1096
7. Uddin MN, Marc Lebel R, Wilman AH. Transverse relaxometry with reduced echo train lengths via stimulated echo compensation. *Magn Reson Med* 2013; 70:1340–1346
8. Coolen BF, Simonis FF, Geelen T, et al. Quantitative T2 mapping of the mouse heart by segmented MLEV phase-cycled T2 preparation. *Magn Reson Med* 2014; 72:409–417
9. Baeßler B, Schaarschmidt F, Stehning C, Schnackenburg B, Maintz D, Bunck AC. Cardiac T2-mapping using a fast gradient echo spin echo sequence: first in vitro and in vivo experience. *J Cardiovasc Magn Reson* 2015; 17:67
10. Joseph GB, McCulloch CE, Nevitt MC, et al. A reference database of cartilage 3 T MRI T2 values in knees without diagnostic evidence of cartilage degeneration: data from the osteoarthritis initiative. *Osteoarthritis Cartilage* 2015; 23:897–905
11. Kaneko Y, Nozaki T, Yu H, et al. Normal T2 map profile of the entire femoral cartilage using an angle/layer-dependent approach. *J Magn Reson Imaging* 2015; 42:1507–1516
12. Chang EY, Ma Y, Du J. MR parametric mapping as a biomarker of early joint degeneration. *Sports Health* 2016; 8:405–411
13. Crema MD, Roemer FW, Marra MD, et al. Articular cartilage in the knee: current MR imaging techniques and applications in clinical practice and research. *RadioGraphics* 2011; 31:37–61
14. Endo J, Watanabe A, Sasho T, et al. Utility of T2 mapping and dGEMRIC for evaluation of cartilage repair after allograft chondrocyte implantation in a rabbit model. *Osteoarthritis Cartilage* 2015; 23:280–288
15. Nishii T, Shiomi T, Tanaka H, Yamazaki Y, Murase K, Sugano N. Loaded cartilage T2 mapping in patients with hip dysplasia. *Radiology* 2010; 256:955–965
16. Dunn TC, Lu Y, Jin H, Ries MD, Majumdar S. T2 relaxation time of cartilage at MR imaging: comparison with severity of knee osteoarthritis. *Radiology* 2004; 232:592–598
17. Zhong H, Miller DJ, Urish KL. T2 map signal variation predicts symptomatic osteoarthritis progression: data from the Osteoarthritis Initiative. *Skeletal Radiol* 2016; 45:909–913
18. Mosher TJ, Dardzinski BJ. Cartilage MRI T2 relaxation time mapping: overview and applications. *Semin Musculoskelet Radiol* 2004; 8:355–368
19. White LM, Sussman MS, Hurtig M, Probyn L, Tomlinson G, Kandel R. Cartilage T2 assessment: differentiation of normal hyaline cartilage and reparative tissue after arthroscopic cartilage repair in equine subjects. *Radiology* 2006; 241:407–414
20. Kim HK, Serai S, Lindquist D, et al. Quantitative skeletal muscle MRI. Part 2. MR spectroscopy and T2 relaxation time mapping: comparison between boys with Duchenne muscular dystrophy and healthy boys. *AJR* 2015; 205:[web]W216–W223
21. Azzabou N, Loureiro de Sousa P, Caldas E, Carlier PG. Validation of a generic approach to muscle water T2 determination at 3T in fat-infiltrated skeletal muscle. *J Magn Reson Imaging* 2015; 41:645–653
22. Klupp E, Weidlich D, Schlaeger S, et al. B1-insensitive T2 mapping of healthy thigh muscles using a T2-prepared 3D TSE sequence. *PLoS One* 2017; 12:e0171337
23. Huang Y, Majumdar S, Genant HK, et al. Quantitative MR relaxometry study of muscle composition and function in Duchenne muscular dystrophy. *J Magn Reson Imaging* 1994; 4:59–64
24. Maillard SM, Jones R, Owens C, et al. Quantitative assessment of MRI T2 relaxation time of thigh muscles in juvenile dermatomyositis. *Rheumatology (Oxford)* 2004; 43:603–608
25. Patten C, Meyer RA, Fleckenstein JL. T2 mapping of muscle. *Semin Musculoskelet Radiol* 2003; 7:297–305
26. Arpan I, Forbes SC, Lott DJ, et al. T_2 mapping provides multiple approaches for the characterization of muscle involvement in neuromuscular diseases: a cross-sectional study of lower leg muscles in 5-15-year-old boys with Duchenne muscular dystrophy. *NMR Biomed* 2013; 26:320–328
27. Wokke BH, Van Den Bergen JC, Hooijmans MT, Verschuuren JJ, Niks EH, Kan HE. T2 relaxation times are increased in skeletal muscle of DMD but not BMD patients. *Muscle Nerve* 2016; 53:38–43
28. Ploutz-Snyder LL, Nyren S, Cooper TG, Potchen EJ, Meyer RA. Different effects of exercise and edema on T2 relaxation in skeletal muscle. *Magn Reson Med* 1997; 37:676–682
29. Akella SV, Regatte RR, Gougoutas AJ, et al. Proteoglycan-induced changes in $T_{1\rho}$-relaxation of articular cartilage at 4T. *Magn Reson Med* 2001; 46:419–423
30. Li X, Benjamin Ma C, Link TM, et al. *In vivo* $T_{1\rho}$ and T_2 mapping of articular cartilage in osteoarthritis of the knee using 3 T MRI. *Osteoarthritis Cartilage* 2007; 15:789–797
31. Wang L, Regatte RR. $T_{1\rho}$ MRI of human musculoskeletal system. *J Magn Reson Imaging* 2015; 41:586–600
32. Casula V, Nissi MJ, Podlipská J, et al. Elevated adiabatic $T_{1\rho}$ and $T_{2\rho}$ in articular cartilage are associated with cartilage and bone lesions in early osteoarthritis: a preliminary study. *J Magn Reson Imaging* 2017; 46:678–689
33. Hänninen N, Rautiainen J, Rieppo L, Saarakkala S, Nissi MJ. Orientation anisotropy of quantitative MRI relaxation parameters in ordered tissue. *Sci Rep* 2017; 7:9606
34. Duvvuri U, Charagundla SR, Kudchodkar SB, et al. Human knee: in vivo $T1_{\rho}$-weighted MR imaging at 1.5 T—preliminary experience. *Radiology* 2001; 220:822–826
35. Pakin SK, Xu J, Schweitzer ME, Regatte RR. Rapid 3D-$T_{1\rho}$ mapping of the knee joint at 3.0T with parallel imaging. *Magn Reson Med* 2006; 56:563–571
36. Tsushima H, Okazaki K, Takayama Y, et al. Evaluation of cartilage degradation in arthritis using T1ρ magnetic resonance imaging mapping. *Rheumatol Int* 2012; 32:2867–2875
37. Keenan KE, Besier TF, Pauly JM, et al. Prediction of glycosaminoglycan content in human cartilage by age, T1ρ and T2 MRI. *Osteoarthritis Cartilage* 2011; 19:171–179
38. Nozaki T, Kaneko Y, Yu HJ, Kaneshiro K, Schwarzkopf R, Yoshioka H. Comparison of T1rho imaging between spoiled gradient echo (SPGR) and balanced steady state free precession (b-FFE) sequence of knee cartilage at 3T MRI. *Eur J Radiol* 2015; 84:1299–1305

39. Yoon MA, Hong SJ, Im AL, Kang CH, Kim BH, Kim IS. Comparison of T1rho and T2 mapping of knee articular cartilage in an asymptomatic population. *Korean J Radiol* 2016; 17:912–918
40. Chen W. Errors in quantitative T1rho imaging and the correction methods. *Quant Imaging Med Surg* 2015; 5:583–591
41. van Tiel J, Bron EE, Tiderius CJ, et al. Reproducibility of 3D delayed gadolinium enhanced MRI of cartilage (dGEMRIC) of the knee at 3.0 T in patients with early stage osteoarthritis. *Eur Radiol* 2013; 23:496–504
42. Burstein D, Velyvis J, Scott KT, et al. Protocol issues for delayed Gd(DTPA)$^{2-}$-enhanced MRI (dGEMRIC) for clinical evaluation of articular cartilage. *Magn Reson Med* 2001; 45:36–41
43. Crema MD, Hunter DJ, Burstein D, et al. Association of changes in delayed gadolinium-enhanced MRI of cartilage (dGEMRIC) with changes in cartilage thickness in the medial tibiofemoral compartment of the knee: a 2 year follow-up study using 3.0 T MRI. *Ann Rheum Dis* 2014; 73:1935–1941
44. Neuman P, Tjörnstrand J, Svensson J, et al. Longitudinal assessment of femoral knee cartilage quality using contrast enhanced MRI (dGEMRIC) in patients with anterior cruciate ligament injury: comparison with asymptomatic volunteers. *Osteoarthritis Cartilage* 2011; 19:977–983
45. Zilkens C, Holstein A, Bittersohl B, et al. Delayed gadolinium-enhanced magnetic resonance imaging of cartilage in the long-term follow-up after Perthes disease. *J Pediatr Orthop* 2010; 30:147–153
46. Vasiliadis HS, Danielson B, Ljungberg M, McKeon B, Lindahl A, Peterson L. Autologous chondrocyte implantation in cartilage lesions of the knee: long-term evaluation with magnetic resonance imaging and delayed gadolinium-enhanced magnetic resonance imaging technique. *Am J Sports Med* 2010; 38:943–949
47. Fleming BC, Oksendahl HL, Mehan WA, et al. Delayed gadolinium-enhanced MR imaging of cartilage (dGEMRIC) following ACL injury. *Osteoarthritis Cartilage* 2010; 18:662–667
48. Watanabe A, Obata T, Ikehira H, Ueda T, Moriya H, Wada Y. Degeneration of patellar cartilage in patients with recurrent patellar dislocation following conservative treatment: evaluation with delayed gadolinium-enhanced magnetic resonance imaging of cartilage. *Osteoarthritis Cartilage* 2009; 17:1546–1553
49. Salo EN, Nissi MJ, Kulmala KA, Tiitu V, Töyräs J, Nieminen MT. Diffusion of Gd-DTPA^{2-} into articular cartilage. *Osteoarthritis Cartilage* 2012; 20:117–126
50. Fayad LM, Jacobs MA, Wang X, Carrino JA, Bluemke DA. Musculoskeletal tumors: how to use anatomic, functional, and metabolic MR techniques. *Radiology* 2012; 265:340–356
51. Hsieh TJ, Jaw TS, Chuang HY, Jong YJ, Liu GC, Li CW. Muscle metabolism in Duchenne muscular dystrophy assessed by in vivo proton magnetic resonance spectroscopy. *J Comput Assist Tomogr* 2009; 33:150–154
52. Fayad LM, Salibi N, Wang X, et al. Quantification of muscle choline concentrations by proton MR spectroscopy at 3 T: technical feasibility. *AJR* 2010; 194:[web]W73–W79
53. Wang CK, Li CW, Hsieh TJ, Chien SH, Liu GC, Tsai KB. Characterization of bone and soft-tissue tumors with in vivo ^{1}H MR spectroscopy: initial results. *Radiology* 2004; 232:599–605
54. Takashima H, Takebayashi T, Ogon I, et al. Analysis of intra and extramyocellular lipids in the multifidus muscle in patients with chronic low back pain using MR spectroscopy. *Br J Radiol* 2018; 91:20170536
55. Bredella MA, Ghomi RH, Thomas BJ, Miller KK, Torriani M. Comparison of 3.0 T proton magnetic resonance spectroscopy short and long echo-time measures of intramyocellular lipids in obese and normal-weight women. *J Magn Reson Imaging* 2010; 32:388–393
56. Fischmann A, Hafner P, Gloor M, et al. Quantitative MRI and loss of free ambulation in Duchenne muscular dystrophy. *J Neurol* 2013; 260:969–974
57. Mengiardi B, Schmid MR, Boos N, et al. Fat content of lumbar paraspinal muscles in patients with chronic low back pain and in asymptomatic volunteers: quantification with MR spectroscopy. *Radiology* 2006; 240:786–792
58. Pfirrmann CW, Schmid MR, Zanetti M, Jost B, Gerber C, Hodler J. Assessment of fat content in supraspinatus muscle with proton MR spectroscopy in asymptomatic volunteers and patients with supraspinatus tendon lesions. *Radiology* 2004; 232:709–715
59. Torriani M, Townsend E, Thomas BJ, Bredella MA, Ghomi RH, Tseng BS. Lower leg muscle involvement in Duchenne muscular dystrophy: an MR imaging and spectroscopy study. *Skeletal Radiol* 2012; 41:437–445
60. Wang X, Salibi N, Fayad LM, Barker PB. Proton magnetic resonance spectroscopy of skeletal muscle: a comparison of two quantitation techniques. *J Magn Reson* 2014; 243:81–84
61. Johnston JH, Kim HK, Merrow AC, et al. Quantitative skeletal muscle MRI. Part 1. Derived T2 fat map in differentiation between boys with Duchenne muscular dystrophy and healthy boys. *AJR* 2015; 205:[web]W207–W215
62. Karampinos DC, Yu H, Shimakawa A, Link TM, Majumdar S. T_1-corrected fat quantification using chemical shift-based water/fat separation: application to skeletal muscle. *Magn Reson Med* 2011; 66:1312–1326
63. Reeder SB, Hu HH, Sirlin CB. Proton density fat-fraction: a standardized MR-based biomarker of tissue fat concentration. *J Magn Reson Imaging* 2012; 36:1011–1014
64. Dixon WT. Simple proton spectroscopic imaging. *Radiology* 1984; 153:189–194
65. Burakiewicz J, Sinclair CDJ, Fischer D, Walter GA, Kan HE, Hollingsworth KG. Quantifying fat replacement of muscle by quantitative MRI in muscular dystrophy. *J Neurol* 2017; 264:2053–2067
66. Wokke BH, van den Bergen JC, Versluis MJ, et al. Quantitative MRI and strength measurements in the assessment of muscle quality in Duchenne muscular dystrophy. *Neuromuscul Disord* 2014; 24:409–416
67. Gaeta M, Scribano E, Mileto A, et al. Muscle fat fraction in neuromuscular disorders: dual-echo dual-flip-angle spoiled gradient-recalled MR imaging technique for quantification—a feasibility study. *Radiology* 2011; 259:487–494
68. Hiba B, Richard N, Hébert LJ, et al. Quantitative assessment of skeletal muscle degeneration in patients with myotonic dystrophy type 1 using MRI. *J Magn Reson Imaging* 2012; 35:678–685
69. Willis TA, Hollingsworth KG, Coombs A, et al. Quantitative muscle MRI as an assessment tool for monitoring disease progression in LGMD2I: a multicentre longitudinal study. *PLoS One* 2013; 8:e70993
70. Liu CY, McKenzie CA, Yu H, Brittain JH, Reeder SB. Fat quantification with IDEAL gradient echo imaging: correction of bias from T_1 and noise. *Magn Reson Med* 2007; 58:354–364
71. Schlaeger S, Freitag F, Klupp E, et al. Thigh muscle segmentation of chemical shift encoding-based water-fat magnetic resonance images: the reference database MyoSegmenTUM. *PLoS One* 2018; 13:e0198200
72. Le Bihan D, Breton E, Lallemand D, Grenier P, Cabanis E, Laval-Jeantet M. MR imaging of intravoxel incoherent motions: application to diffusion and perfusion in neurologic disorders. *Radiology* 1986; 161:401–407
73. Yanagisawa O, Shimao D, Maruyama K, Nielsen M, Irie T, Niitsu M. Diffusion-weighted magnetic resonance imaging of human skeletal muscles: gender-, age- and muscle-related differences in apparent diffusion coefficient. *Magn Reson Imaging* 2009; 27:69–78
74. Huisman TA. Diffusion-weighted and diffusion tensor imaging of the brain, made easy. *Cancer Imaging* 2010; 10(spec no A):S163–S171
75. Chilla GS, Tan CH, Xu C, Poh CL. Diffusion weighted magnetic resonance imaging and its recent trend: a survey. *Quant Imaging Med Surg* 2015; 5:407–422
76. Froeling M, Oudeman J, Strijkers GJ, et al. Muscle changes detected with diffusion-tensor imag-

ing after long-distance running. *Radiology* 2015; 274:548–562
77. Van Donkelaar CC, Kretzers LJ, Bovendeerd PH, et al. Diffusion tensor imaging in biomechanical studies of skeletal muscle function. *J Anat* 1999; 194:79–88
78. Pierpaoli C, Basser PJ. Toward a quantitative assessment of diffusion anisotropy. *Magn Reson Med* 1996; 36:893–906
79. Zaraiskaya T, Kumbhare D, Noseworthy MD. Diffusion tensor imaging in evaluation of human skeletal muscle injury. *J Magn Reson Imaging* 2006; 24:402–408
80. Oudeman J, Nederveen AJ, Strijkers GJ, Maas M, Luijten PR, Froeling M. Techniques and applications of skeletal muscle diffusion tensor imaging: a review. *J Magn Reson Imaging* 2016; 43:773–788
81. Chang EY, Du J, Chung CB. UTE imaging in the musculoskeletal system. *J Magn Reson Imaging* 2015; 41:870–883
82. Chen B, Zhao Y, Cheng X, et al. Three-dimensional ultrashort echo time cones (3D UTE-Cones) magnetic resonance imaging of entheses and tendons. *Magn Reson Imaging* 2018; 49:4–9
83. Kijowski R, Wilson JJ, Liu F. Bicomponent ultrashort echo time T2* analysis for assessment of patients with patellar tendinopathy. *J Magn Reson Imaging* 2017; 46:1441–1447
84. Manhard MK, Horch RA, Gochberg DF, Nyman JS, Does MD. In vivo quantitative MR imaging of bound and pore water in cortical bone. *Radiology* 2015; 277:221–229
85. Nazaran A, Carl M, Ma Y, et al. Three-dimensional adiabatic inversion recovery prepared ultrashort echo time cones (3D IR-UTE-Cones) imaging of cortical bone in the hip. *Magn Reson Imaging* 2017; 44:60–64
86. Williams A, Qian Y, Bear D, Chu CR. Assessing degeneration of human articular cartilage with ultra-short echo time (UTE) T2* mapping. *Osteoarthritis Cartilage* 2010; 18:539–546
87. Fouré A. New imaging methods for non-invasive assessment of mechanical, structural, and biochemical properties of human Achilles tendon: a mini review. *Front Physiol* 2016; 7:324
88. Wang N, Xia Y. Anisotropic analysis of multicomponent T_2 and $T_{1\rho}$ relaxations in Achilles tendon by NMR spectroscopy and microscopic MRI. *J Magn Reson Imaging* 2013; 38:625–633
89. Juras V, Apprich S, Szomolanyi P, Bieri O, Deligianni X, Trattnig S. Bi-exponential T2* analysis of healthy and diseased Achilles tendons: an in vivo preliminary magnetic resonance study and correlation with clinical score. *Eur Radiol* 2013; 23:2814–2822
90. Liu F, Kijowski R. Assessment of different fitting methods for *in-vivo* bi-component T2* analysis of human patellar tendon in magnetic resonance imaging. *Muscles Ligaments Tendons J* 2017; 7:163–172
91. Bae WC, Dwek JR, Znamirowski R, et al. Ultrashort echo time MR imaging of osteochondral junction of the knee at 3 T: identification of anatomic structures contributing to signal intensity. *Radiology* 2010; 254:837–845
92. Du J, Carl M, Bae WC, et al. Dual inversion recovery ultrashort echo time (DIR-UTE) imaging and quantification of the zone of calcified cartilage (ZCC). *Osteoarthritis Cartilage* 2013; 21:77–85
93. Gold GE, Chen CA, Koo S, Hargreaves BA, Bangerter NK. Recent advances in MRI of articular cartilage. *AJR* 2009; 193:628–638
94. Williams AA, Titchenal MR, Do BH, Guha A, Chu CR. MRI UTE-T2* shows high incidence of cartilage subsurface matrix changes 2 years after ACL reconstruction. *J Orthop Res* 2018 Jul 20 [Epub ahead of print]
95. Chu CR, Williams AA, West RV, et al. Quantitative magnetic resonance imaging UTE-T2* mapping of cartilage and meniscus healing after anatomic anterior cruciate ligament reconstruction. *Am J Sports Med* 2014; 42:1847–1856
96. Shao H, Chang EY, Pauli C, et al. UTE bi-component analysis of T2* relaxation in articular cartilage. *Osteoarthritis Cartilage* 2016; 24:364–373
97. Chen J, Grogan SP, Shao H, et al. Evaluation of bound and pore water in cortical bone using ultrashort-TE MRI. *NMR Biomed* 2015; 28:1754–1762
98. Horch RA, Gochberg DF, Nyman JS, Does MD. Clinically compatible MRI strategies for discriminating bound and pore water in cortical bone. *Magn Reson Med* 2012; 68:1774–1784
99. Williams A, Qian Y, Chu CR. UTE-T2* mapping of human articular cartilage in vivo: a repeatability assessment. *Osteoarthritis Cartilage* 2011; 19:84–88
100. Berendsen HJC. Nuclear magnetic resonance study of collagen hydration. *J Chem Phys* 1962; 36:3297–3305
101. Chang EY, Du J, Bae WC, Chung CB. Qualitative and quantitative ultrashort echo time imaging of musculoskeletal tissues. *Semin Musculoskelet Radiol* 2015; 19:375–386
102. Ma YJ, Chang EY, Carl M, Du J. Quantitative magnetization transfer ultrashort echo time imaging using a time-efficient 3D multispoke Cones sequence. *Magn Reson Med* 2018; 79:692–700
103. Ma YJ, Shao H, Du J, Chang EY. Ultrashort echo time magnetization transfer (UTE-MT) imaging and modeling: magic angle independent biomarkers of tissue properties. *NMR Biomed* 2016; 29:1546–1552
104. Zhu Y, Cheng X, Ma Y, et al. Rotator cuff tendon assessment using magic-angle insensitive 3D ultrashort echo time cones magnetization transfer (UTE-Cones-MT) imaging and modeling with histological correlation. *J Magn Reson Imaging* 2018; 48:160–168
105. Chang EY, Bae WC, Shao H, et al. Ultrashort echo time magnetization transfer (UTE-MT) imaging of cortical bone. *NMR Biomed* 2015; 28:873–880
106. Ma YJ, Tadros A, Du J, Chang EY. Quantitative two-dimensional ultrashort echo time magnetization transfer (2D UTE-MT) imaging of cortical bone. *Magn Reson Med* 2018; 79:1941–1949

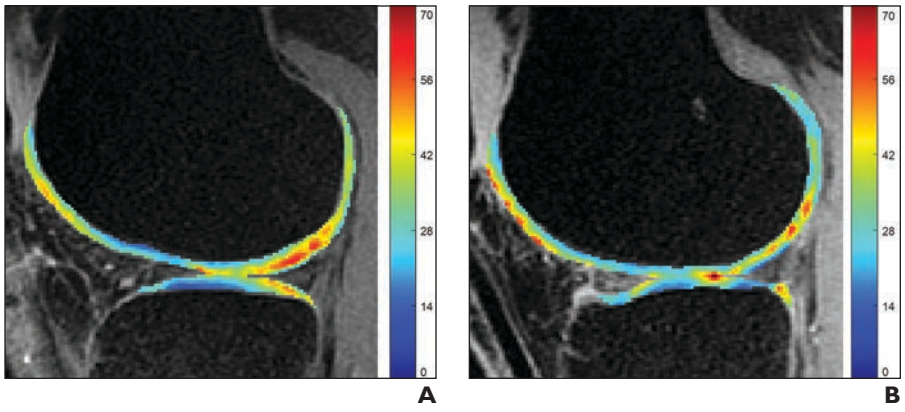

Fig. 1—Two subjects who underwent 2D multiecho spin-echo T2-weighted MRI of knee (TE = 6.1, 12.2, 18.3, 24.4, 30.4, 36.5, 42.6, 48.7, 54.8, 60.9, 67.0, and 73.1 ms).
A, 43-year-old male volunteer with no symptoms. Image shows highest T2 values in posterior weight-bearing aspect of medial femoral condyle, which is at magic angle. Color scale denotes T2 values.
B, 67-year-old woman with knee osteoarthritis. Osteoarthritis of knee was determined by clinical examination and radiographs. There are irregular areas of high T2 values at femoral trochlea, posterior weight-bearing aspect of medial femoral condyle, and medial tibial plateau, indicating areas of abnormal cartilage. Color scale denotes T2 values.

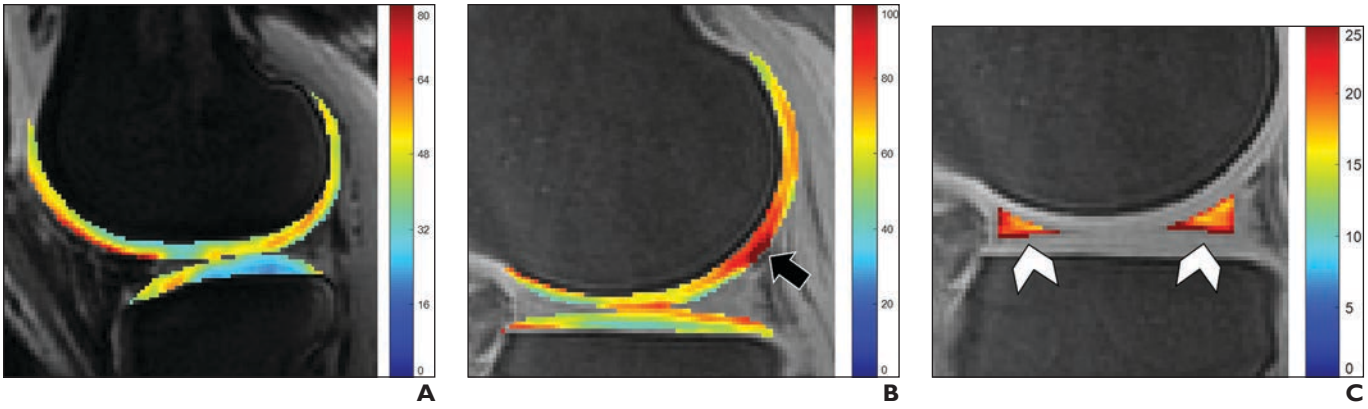

Fig. 2—70-year-old woman without symptoms.
A, T1ρ measurement obtained with conventional MRI technique with longer TE (10 ms) can be used to evaluate cartilage. Color scale denotes T1ρ values.
B and **C,** Using ultrashort TE (UTE) (0.032 ms), additional information is obtained from short T2 components. High signal intensity at posterior portion of medial femoral condyle (*arrow*, **B**) suggests loss of proteoglycan. In addition, using UTE technique, T1ρ measurements can be obtained from tissues with short mean T2 values, such as menisci (*arrowheads*, **C**). Sequences used were 2D spiral T1ρ measurement (time to spin lock [TSL] = 0, 20, 40, and 80 ms) and 3D UTE-Cones T1ρ measurement (TSL = 0, 5, 10, and 20 ms). Color scales denote T1ρ values.

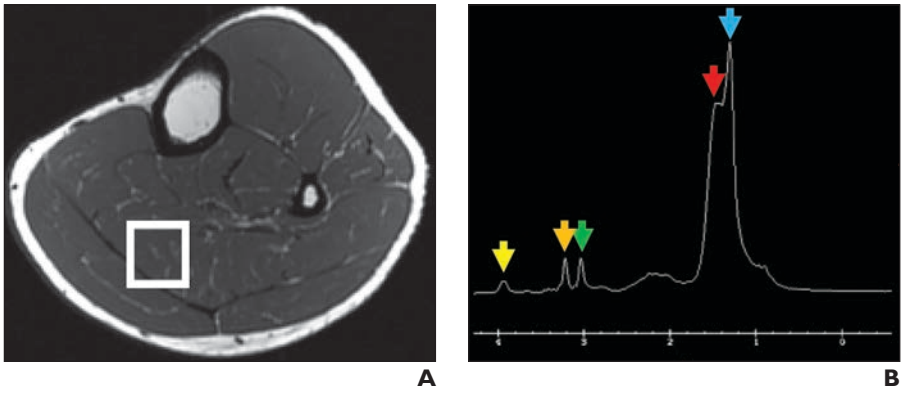

Fig. 3—28-year-old man without symptoms.
A and **B,** T1-weighted MRI (**A**) shows voxel location (*square*) used for MR spectroscopy. Graph (**B**) shows corresponding water-suppressed spectrum from that region. Lipids dominate signal in this region with distinct peaks from CH_2 groups on extra- and intramyocellular lipids (*red* and *blue arrows*, respectively). Distinct peak from trimethylamine is visible (*orange arrow*), as are peaks from CH_3 and CH_2 groups of creatine (*green* and *yellow arrows*, respectively). Numbers on graph axis denote frequency (ppm).

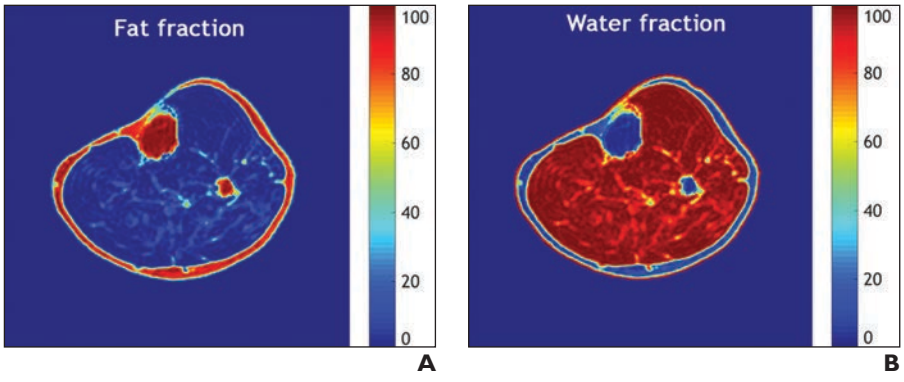

Fig. 4—28-year-old man without symptoms.
A and **B,** Chemical-shift imaging was performed to generate fat (**A**) and water (**B**) fraction maps, which allow quantification of skeletal muscle. Low fat and high water fractions in musculature of leg in this volunteer are normal.

Fig. 5—54-year-old male cadaveric specimen with osteoarthritis.
A and **B,** Ultrashort-TE MRI highlights deep layers of articular cartilage of medial femorotibial compartment (**A**) and at femoral trochlea (**B**). Abnormal areas, represented by missing bright lines, can be identified on weight-bearing medial femoral condyle (*thick arrow*, **A**), medial tibial plateau (*thin arrow*, **A**), and patella (*arrowhead*, **B**). Subtle areas (*red lines*) can also be quantified.
C, Graphs show TE times for femoral condyle (*top*) and femoral trochlea (*bottom*).

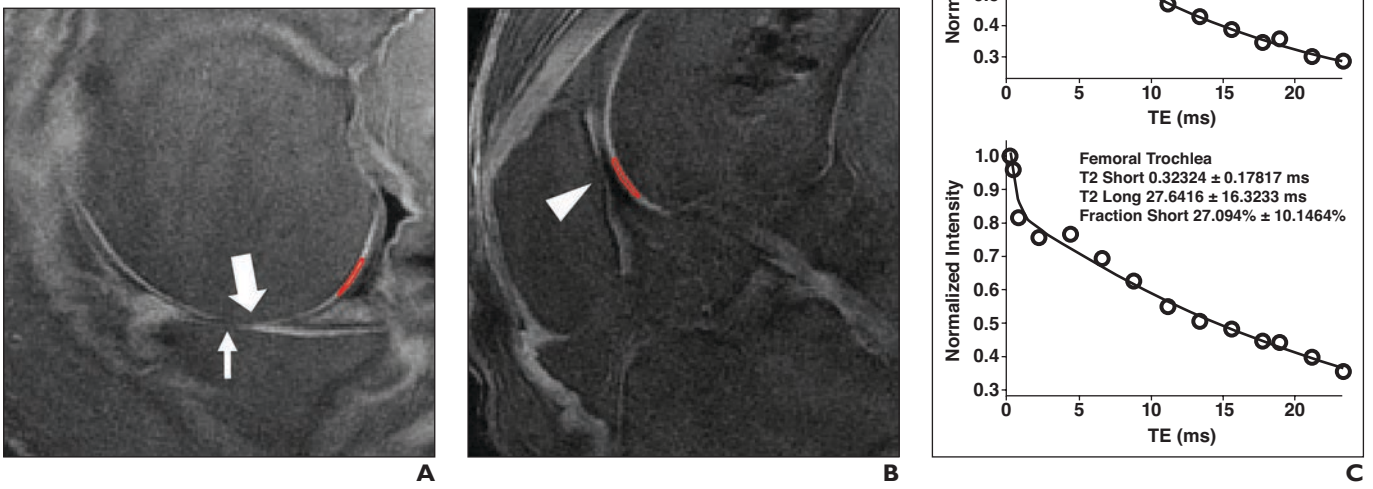

Fig. 6—Two subjects who underwent shoulder imaging.
A and **B,** 25-year-old man with intermittent shoulder pain. Coronal oblique ultrashort-TE (UTE) magnetization transfer (MT) image of supraspinatus tendon with macromolecular map (**A**) shows low macromolecular fraction, as denoted by color scale on right, suggesting tendinopathy. Graph of fitting curves from two-pool MT modeling (**B**) shows excellent fit, with mean macromolecular fraction (f) of 12.7% ± 1.0%.
C and **D,** 33-year-old woman without symptoms. Coronal oblique UTE MT image of supraspinatus tendon with macromolecular map (**C**) shows high macromolecular fraction, as denoted by color scale on right. Graph of fitting curves from two-pool MT modeling (**D**) shows excellent fit, with mean macromolecular fraction (f) of 13.8% ± 0.9%. This technique enables acquisition of macromolecular fractions that are much less sensitive to magic angle effects.

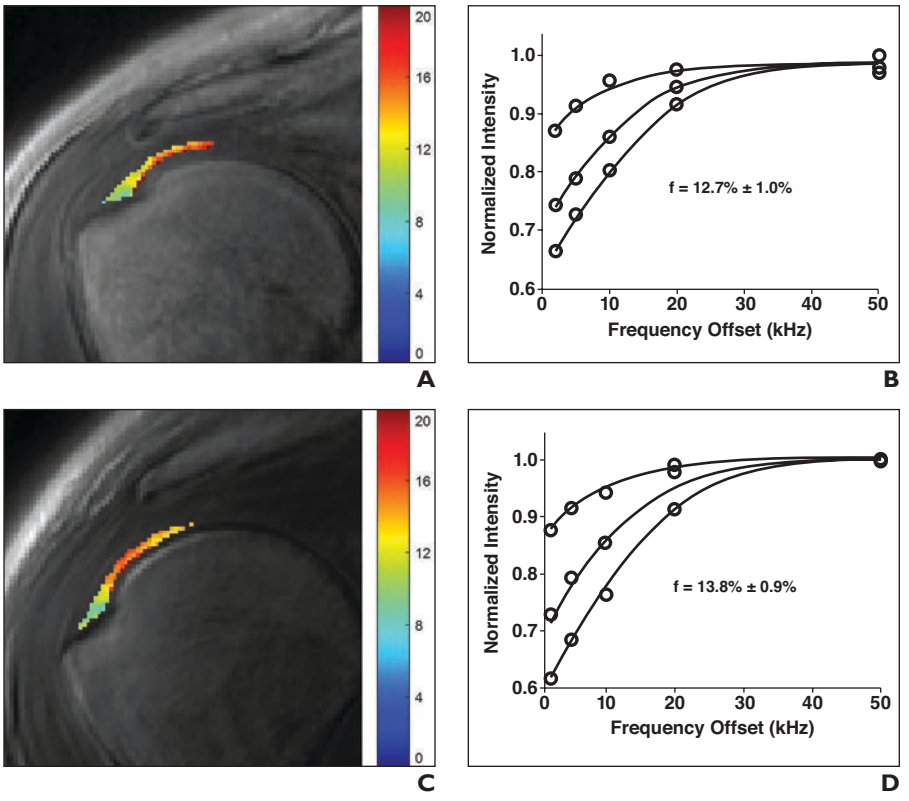

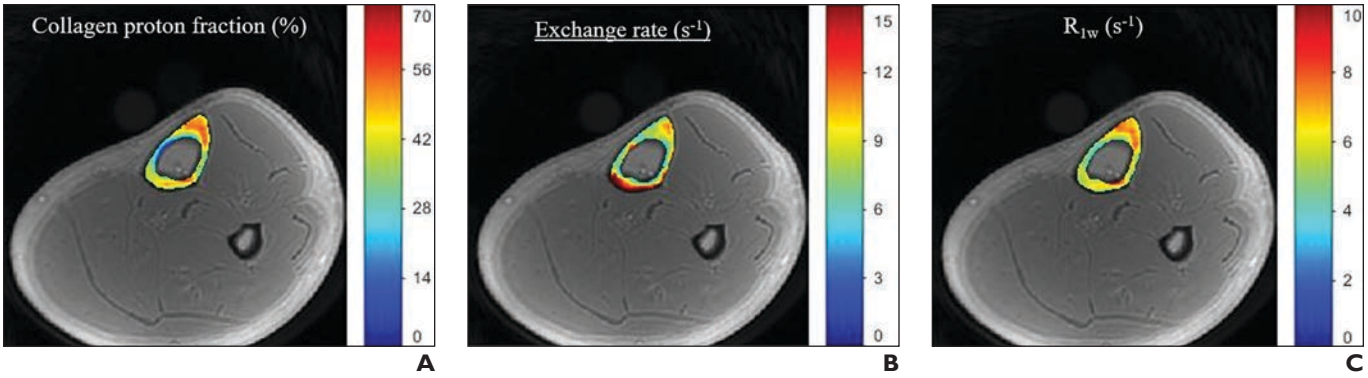

Fig. 7—35-year-old man without symptoms.
A–C, Ultrashort-TE (UTE) magnetization transfer (MT) images of left leg provide color mapping with quantification information of tibial cortical bone, including macromolecular fraction (**A**), proton exchange rate from macromolecular to water pools (**B**), and spin-lattice relaxation rate of water pool (R_{1w}; **C**). Color bars indicate gradation of MT measures, and regional variations can be seen in different portions of tibial cortex, reflecting compositional and structural differences. For UTE-Cones MT modeling, flip angle was 500°, 1000°, and 1500°, and frequency offset was 2, 5, 10, 20, and 50 kHz. For UTE-Cones T1 measurement for MT modeling, actual flip angle was 45° and TR was 20 and 100 ms; with variable TR, flip angle was 45° and TR was 20, 50, and 150 ms.